TERN airborne LiDAR and hyperspectral products document

26 November 2018

Albert van Dijk[1], Matt Paget[2], Lola Suárez[3], Matt Gale[1]

[1] Centre for Water and Landscape Dynamics, Australian National University
[2] Oceans and Atmosphere, CSIRO
[3] Department of Infrastructure Engineering, University of Melbourne

Centre for Water and Landscape Dynamics
Fenner School of Environment & Society
Australian National University

Last updated 26 November 2018

Cite as: Van Dijk, A.I.J.M., Paget, M., Suarez, L., Gale, M. (2018) *TERN airborne LiDAR and hyperspectral products document*. Australian National University, Canberra, 27 pp.

TABLE OF CONTENTS

LIST OF ABBREVIATIONS

ACT	Australian Capital Territory
Ali	Alice Mulga site
ANU	Australian National University
ARA	Airborne Research Australia
ASCII	American Standard Code for Information Interchange
CA	Coastal Aerosol
CBH	overstorey Canopy Base Height
Cho	Chowilla site
CLI	Canopy Layering Index
Cre	Credo site
CSIRO	Commonwealth Science and Industrial Research Organisation
CTH	overstorey Canopy Top Height
DEM	Digital Elevation Model
EVI	Enhanced Vegetation Index
FBF	Fraction Building Footprints
Fow	Fowler's Gap site
FPAR	Fraction Absorbed Photosynthetically Active Radiation
FWF	Full-Wave Form LiDAR
GeoTIFF	Geostationary Earth Orbit Tagged Image File Format
GVMI	Global Vegetation Moisture Index
HDF	Hierarchical Data Format
HPC	High-Performance Computing
Inj	Injune site
Kar	Karawatha site
Kc	crop coefficient
LAI	Leaf Area Index
LAS	LASer file exchange format
LCF	vegetation Layer Cover Fraction
LiDAR	Light Detection And Ranging
Lit	Litchfield site
MODIS	Moderate Resolution Imaging Spectroradiometer
NDVI	Normalised Difference Vegetation Index
NetCDF	Network Common Data Form
NIR	Near Infra-Red
OLI	Landsat 8 Operational Land Imager
OWL	Open Water Likelihood
PMSC	Penman-Monteith Surface Conductance
QA/QC	Quality Assurance / Quality Control
RMI	Residual Moisture Index
RMIT	Royal Melbourne Institute of Technology
RMSE	Root Mean Square Error
Rob	Robson site
Rus	Rushworth site
Sam	Samford site
SWIR	Short-Wave Infra-Red
TERN	Terrestrial Ecosystem Research Network
Tum	Tumbarumba site
VCF	Vegetation Cover Fraction
VH	Vegetation Height
VI	Vegetation Index
VIR	Visual and Infra-Red
VIS	VISible
War	Warra site
Wat	Watts Creek site
Wyn	Wynnum mangrove site
Zig	Zig Zag Creek site

ACKNOWLEDGEMENTS

The authors would like to acknowledge all individuals involved in data collection, product specification and report review. They include

- Adam Leavesley, Greg Baines and Jennifer Smits (ACT Parks & Conservation);
- Adam Steer, Ben Scheele, Cris Brack, Kara Youngentob, Marta Yebra, Phil Gibbons and Rowena Smith (Australian National University);
- Alex Held, Arancha Cabello-Leblic and Michael Schaeffer (CSIRO);
- Stefan Maier (Maitec);
- Simon Jones (Royal Melbourne Institute of Technology);
- Arco Lucieer (University of Tasmania);
- Kasper Johansen, Peter Scarth and Stuart Phinn (University and Queensland);
- Phil Wilkes (University College London, UK); and
- James Cleverly (University of Technology Sydney).

1 INTRODUCTION

This document describes gridded products generated from the airborne and ground data acquired by TERN. The products were generated by the ANU Centre for Water and Landscape Dynamics, following an initial data audit, feasibility analysis, and consultation among TERN partners and external stakeholders.

All data products can be viewed in the TERN-ANU Landscape Data Visualiser, which can be accessed via https://maps.tern.org.au or https://anuwald.science/ternanu. Via the website the data can also be downloaded.

2 DATA ACQUISITION AND PREPROCESSING

2.1 LOCATIONS AND DATA COLLECTION

2.1.1 TERN sites

Airborne data were collected at 15 TERN sites between 2011 and 2016. A description of the sites is provided in Table 1, their location is shown in Figure 1, and an illustrative photo of the vegetation at each of the sites is provided in Figure 2[1].

Table 1. Description of TERN sites (source: http://www.auscover.org.au/news-resources/our-field-sites/).

Code	Site name	Site location	Date(s)	Environment
Tum	Tumbarumba	Southeastern New South Wales, 100 km south-west of Canberra	10-14 Jan 2011	Temperate wet sclerophyll eucalypt forest with average tree height of 40 m. *Eucalyptus delegatensis* (alpine ash) was the dominant species. See also http://www.tern-supersites.net.au/supersites/tumb
Cho	Chowilla (Calperum Mallee)	North of the River Murray floodplains near Renmark, South Australia	30 Jan – 3 Feb 2012	Semi-arid mallee ecosystem in dune and swale system, covered with an open mallee woodland upper story with a chenopod and native grass understory. See also http://www.tern-supersites.net.au/supersites/clpm
Wat	Watts Creek	70 km east of Melbourne, Victoria	5-9 Mar, 13-20 Apr, 1-3, 7 May and 9-16 Sep	Open forest with a eucalypt overstorey greater than 40 m. *E. regnans* (mountain ash) was the dominant species.

[1] All material drawn from http://www.auscover.org.au/news-resources/our-field-sites/

Code	Site name	Site location	Date(s)	Environment
			2012	
Rus	Rushworth Forest	120 km north of Melbourne, Victoria	15 Apr, 3-6 May, 31 May and 6 Jun 2012	Open forest of *E. sideroxylon* (red ironbark), *E. macrorhyncha* (red stringybark), *E. polyanthemos* (red box), *E. goniocalyx* (long leaf box) and *E. microcarpa* (grey box).
Zig	Zig Zag Creek	Eastern Victoria 300 km east of Melbourne, Victoria	16-20 Apr 2012	Dominated by shrubby dry forest and damp forest on the upland slopes, wet forest ecosystems restricted to the higher altitudes and grassy woodlands. Grassy dry forest ecosystems were associated with river valleys.
Cre	Credo (Great Western Woodlands)	Great Western Woodland 500 km north-west of Perth, Western Australia	12-18 May 2012	Open woodland inter-dispersed with open, treeless areas. The main vegetation species were *E. salmonophloia* (salmon gum) reaching up to 20 m, and *E. salubris* (gimlet) between 5-10 m, both with little understory. Saltbush and similar shrubs were also prevalent. See also http://www.tern-supersites.net.au/supersites/gwwl
Rob	Robson Creek	Lamb Range in the Wet Tropics World Heritage area 25 km south-west of Cairns, Queensland	9-16 Sep 2012	Upland rainforest region at 700 m elevation. Notophyll vine forest with a tall canopy at around 40 m and high species diversity. See also http://www.tern-supersites.net.au/supersites/fnqr/robson
Sam	Samford	South East Queensland	21 Jan 2013 – 6 Feb 2013	Improved (*Paspalum dilatum*) pasture with tall eucalypt species. See also http://www.tern-supersites.net.au/supersites/seqp
Kar	Karawatha Forest	South East Queensland	21 Jan 2013 – 6 Feb 2013	Bushland with tall eucalypt species and patches of heathlands and *Melaleuca* swamps. See also http://www.tern-supersites.net.au/supersites/seqp
Wyn	Wynnum mangrove	near Brisbane Airport.	21 Jan 2013 – 6 Feb 2013	Within Moreton Bay, with *Avicennia marina* (grey mangrove) being the dominant mangrove species. See also http://www.tern-supersites.net.au/supersites/seqp
Lit	Litchfield	80 km south of Darwin, Northern Territory	27 May – 2 Jun 2013	Savanna, open eucalypt forests, dominated by *E. miniata* (Darwin woollybutt) and *E. tetrodonta* (Darwin stringybark). See also http://www.tern-supersites.net.au/supersites/lfld
Ali	Alice Mulga	165 km north-northwest of Alice Springs, Northern Territory	Not visited yet, but airborne LiDAR collected	*Acacia aneura* (mulga) canopy which was 6.5m tall on average. See also http://www.tern-supersites.net.au/supersites/alic
War	Warra	60 km west/southwest of Hobart, Tasmania	2-6 Feb 2015	Homogenous tall, wet *E. obliqua* (messmate) forest with wet sclerophyll and rainforest understorey. See also http://www.tern-supersites.net.au/supersites/wrra
Inj	Injune	170 km northwest of Roma, central southeast Queensland	17-22 Aug 2015	Low open woodland and open forest ecosystem. Forests with *Eucalyptus* species dominate the more productive soils, and *Acacia harpophylla* (brigalow) occurs on clay soils. Ironbarks were frequent within the open forests. See also https://www.ecosystem.unsw.edu.au/content/landscape-synthesis/remote-sensing/the-injune-landscape-collaborative-project
Fow	Fowler's Gap	110 km north of Broken Hill, NSW	12-15 Sept 2016	Arid rangelands ecosystem within a long-term ecological monitoring research station. See also http://www.fowlersgap.unsw.edu.au .

Figure 1. Map of Australia showing the location of field and airborne campaign sites carried out by TERN since January 2011 (source: http://www.auscover.org.au/news-resources/our-field-sites/).

2.1.2 Australian Capital Territory data

In addition to the TERN sites, TERN co-invested in enhancing the airborne data capture initiated by the ACT Government. Between 2014 and 2016, airborne LiDAR, multispectral, hyperspectral and panchromatic data were captured over either parts or the entire ACT, depending on data type. All data are available to TERN and others under a Creative Commons license. LiDAR data collected in 2014 were not considered here as they were superseded by more complete and higher-density data acquired in 2015. All other data were considered for product derivation.

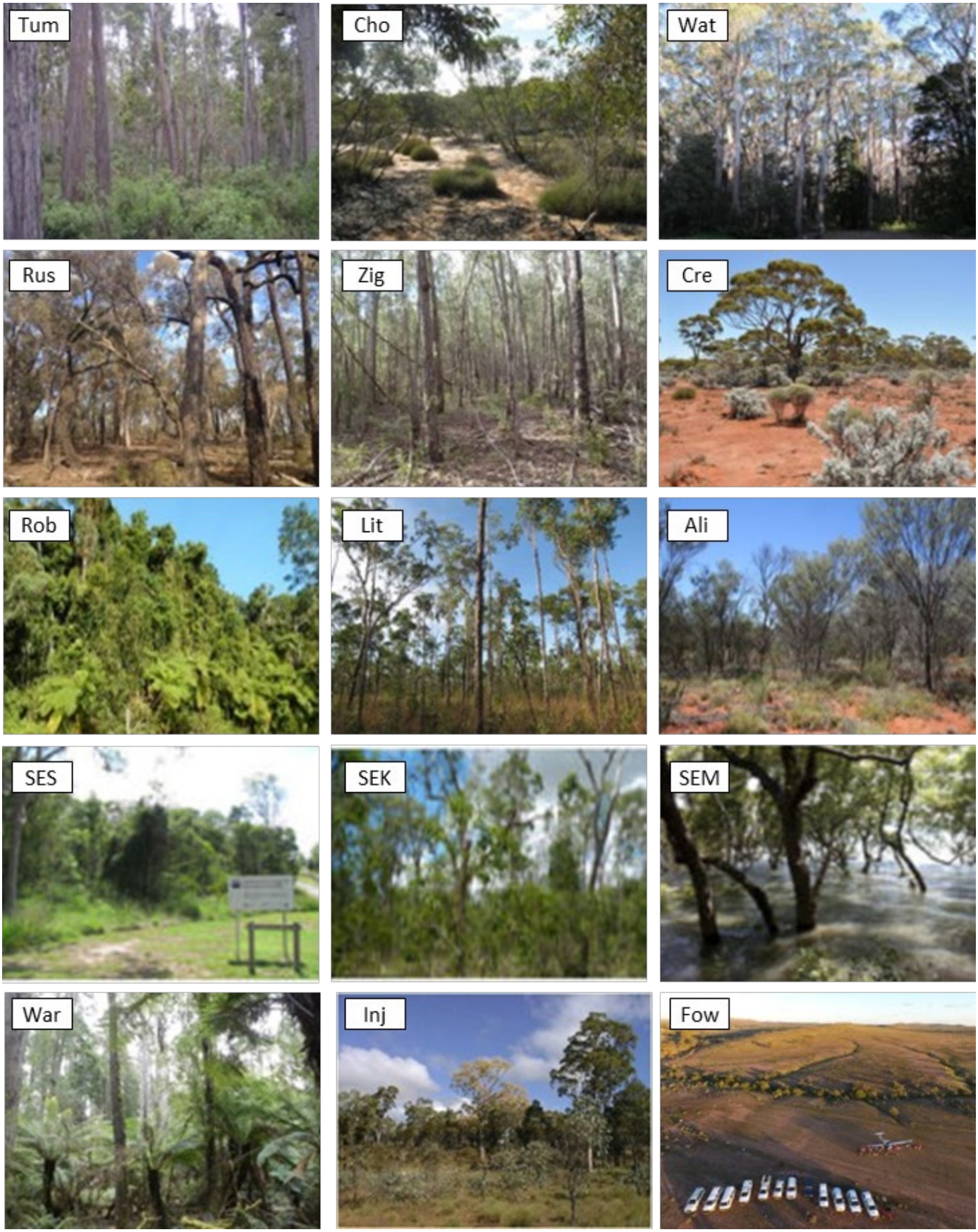

Figure 2. Visual impression of the 15 AusCover sites (for codes see Table 1).

2.2 AIRBORNE LIDAR DATA

An inventory was made of the airborne LiDAR data available via the TERN website and from the ACT Government. The focus was on discrete return LiDAR data. For some of the sites, full-waveform (FWF) LiDAR data was also retained and is available for research. However, it was not considered in the generation of standardised TERN products as at the time of production there was no generally accepted, well-researched and published approach to derive vegetation information from FWF data.

2.2.1 Acquisition

A summary of captured LiDAR data is listed in Table 2. Information was derived from various data reports provided with the data or online (ARA undated, Johansen undated).

Table 2. Characteristics of the LiDAR data captured at the different AusCover sites. DEM=digital elevation model, FWF=full waveform data. The density listed is the nominal density; final densities may vary somewhat.

Code	Date	Density	Format	Operator	DEM	FWF	Comments
Tum	9.1.2011	6 ppm	LAS v?	ARA	✓	×	No data report located
Cho	31.1.2012-1.2.2011	8 ppm	LAS 1.2	ARA	✓	✓	Additional transect
Wat	14.4.2012	8 ppm	LAS 1.2	ARA	✓	✓	
Rus	15.4.2012	8 ppm	LAS 1.2	ARA	✓	✓	
Zig	17.4.2012	8 ppm	LAS 1.2	ARA	✓	✓	
Cre	15.5.2012	8 ppm	LAS 1.2	ARA	✓	✓	
Rob	13-14.9.2012	8 ppm	LAS 1.2	ARA	✓	✓	
Sam	5.10.2013	8 ppm	LAS 1.2	ARA	✓	✓	Two additional transects
Kar	5.10.2013	8 ppm	LAS 1.2	ARA	✓	✓	As above
Wyn	5.10.2013	8 ppm	LAS 1.2	ARA	✓	✓	As above
Lit	1.6.2013	8 ppm	LAS 1.2	ARA	✓	✓	
Ali	20.9.2014		LAS 1.2	ARA	✓	✓	
War	30-31.5.2014		LAS 1.2	ARA	✓	✓	No data report available
Inj	19-20.8.2015		$	ARA	✓	✓	No data report available
ACT	18.05.2015-29.07.2016*	8 ppm	LAS 1.4	RPS	✓	(✓)	FWF for small area only

* some areas were captured at a later date. $ data were corrupted and could not be processed

The LiDAR data captured by ARA was described in a data report (ARA, undated), except for sites *Tum*, *Ali*, *War*, and *Inj*, for which no data report was found. The ARA system included a Riegl Q560 with two GPS systems mounted on an ECO-Dimona research aircraft. ARA reports that "*at a nominal flying height of 300m above ground, the specified footprint of the laser pulse on the ground has a diameter of <0.15m, resulting in an a priori average uncertainty of the horizontal position of any encountered target within this disk of 0.075m*". The following additional surveys, not technically part of the TERN sites but related to it, were also flown by ARA:

- 14 km transect across the Murray River Floodplains near Chowilla (*Cho*) on 31 Jan 2012
- 1 km^2 square region near Whroo, Victoria, on 15 Apr 2012
- 1 x 5 km additional area near Robson Creek (*Rob*) on 14 Sep 2012

- Two transects in Southeast Queensland: from NNW-SSE across Brisbane and from Corinda to Logan River, respectively.

LiDAR data were available as tile LAS files for sites *Tum*, *Ali*, *War* and *Inj*, but no data report or details on their provenance were available. The data for Tumbarumba were further processed and subjected to quality assurance by Chris Hopkinson (visiting scientist at CSIRO). No LiDAR data were available for *Fow*.

LiDAR data over the ACT were captured in 2015 and 2016 by RPS Mapping, with the majority completed between May and June 2015. A Final Report describing the data was available (RPS - Mapping 2016). The total project area captured was approximately 3272 km^2. LiDAR was captured at a nominal density of four pulses per square metre (ppm) across the greater ACT and some surrounding areas, and 8 ppm over Canberra's city centres, with a Trimble AX60 LiDAR system, which contains a Riegl LMS-Q780 laser instrument.

2.2.2 Preprocessing

The LiDAR data collected by ARA were preprocessed as follows (comprehensive details can be found in the ARA data provision report; ARA, unpubl.):

1 Discrete returns were extracted from the raw waveform LiDAR data were processed using the RiAnalyze software.
2 The discrete return data in the scanner coordinate system was combined with the aircraft navigation data to map the returns to the coordinates of the Map Grid of Australia 1994 (MGA94) and Australian Height Datum (AHD) using in-house software.
3 The returns were classified following the LAS version 1.2 standard using LASTools software.
4 The data were resampled to 500-m or 1-km square tiles in two ways: with and without removing data from overlapping scans from subsequent flight lines.
5 A 1-m DEM was generated using LAStools.

The discrete return data were made available in LAS 1.2 format. The data report suggests a likely vertical error of around 0.02 m for ideal conditions (flat target, vertical scan angle) up to 0.15 m in the worst-case scenario.

The ACT LiDAR data were processed in a similar way except for the following: the data were resampled to 2-km square tiles; instead of LASTools the Terrasolid software products (Terrascan and Terramodeler) were used; and the classified, tiled returns were provided in LAS 1.4 format. Raw and decompressed full waveform data were also provided for an area surrounding Black Mountain Reserve. The data report notes that the average pulse density across the ACT was 7.9 ppm, with 8 ppm exceeded even in large areas outside the city centres (despite having a 4 ppm nominal density) and isolated areas with <4 ppm over water bodies and areas of high relief. The vertical accuracy was estimated as better than 0.20 m (1.96 RMSE) for 95% of the returns.

2.3 AIRBORNE HYPERSPECTRAL DATA

An inventory was made of the airborne multi and hyperspectral data available via the TERN website and from the ACT Government.

2.3.1 Acquisition

A summary of captured optical data is provided in Table 3 below. Spatial maps showing data coverage are not shown here but were produced along with the derived products and can be viewed in the TERN-ANU Landscape Data Visualiser.

Table 3. Airborne hyperspectral data acquisitions at the SuperSites. am=morning, pm=afternoon. ? = information not provided

Code	Date	Time	Range	Operator	Conditions	Comments
Tum	7.4.2011		VIR-SWIR	HyMap	?	No data report available
Cho	(31.1.2011-1.2.2011) 24.9.2013[#]	pm	VIR/SWIR	ARA	Clear but severe turbulence	Some data loss
Wat	14.4.2012	pm	VIR/SWIR	ARA	Scattered cumulus shading developing	Some data loss
Rus	15.4.2012	around noon	VIR/SWIR	ARA	Good	
Zig	17.4.2012	around noon	VIR/SWIR	ARA	Cloud shading developing	
Cre	15.5.2012	noon-pm	VIR/SWIR	ARA	Good	2-hour time hiatus due to aircraft issues
Rob	13-14.9.2012	?	VIR/SWIR	ARA	Scattered cloud disappearing	
SES	2.2.2012	?	VIR/SWIR	ARA	?	Two additional transects
Kar	2.2.2012	?	VIR/SWIR	ARA	?	As above
Wyn	2.2.2012	?	VIR/SWIR	ARA	?	As above
Lit	27.5.2013	noon-pm	VIR/SWIR	ARA	Thin cirrus and aerosol	
Ali	–	–	–	–	–	No data available
War	6.2.2015	?	?	?	?	No data report available
Inj	18-19.8.2015	–	–	–	–	No data available
Fow	–	–	–	–	–	No data available
ACT	?	?	VIR-SWIR	Hyvista		No data report found

[#] first data collection failed

Hyperspectral data captured at 10 TERN sites by ARA in 2012 and 2013 were documented in a data report (ARA undated) and the information presented here was derived from that report. For all surveys, the data were collected by two instruments: a SPECIM AisaEAGLE II hyperspectral scanner for the VNIR frequency range and a SPECIM AisaHAWK for the SWIR range. Both were mounted in underwing pods of ARA's ECO-Dimona research aircraft, each one with its own navigation and altitude recorder. The survey areas were the same as described for the LiDAR data with the same additional data collected:

- 14 km transect across the Murray River Floodplains near Chowilla (*Cho*) in the afternoon of 01 Feb 2012 with good conditions but technical issues leading to some data loss.
- 1 km^2 square region near Whroo, Victoria in the afternoon of 15 Apr 2013, under good conditions.
- 1 x 5 km additional area near Robson Creek (*Rob*) on 14 Sep 2012
- Two transects in Southeast Queensland: from NNW-SSE across Brisbane and from Corinda to Logan River, respectively.

With co-investment from CSIRO, HyVista collected hyperspectral data over three parts of the ACT, identified as Mulligans Flat, Black Mountain and Lake Burley Griffin, respectively. The data were collected using a HyMap instrument, with 126 spectral bands spanning the wavelength interval 0.45–2.5 µm (VIS-NIR-SWIR). Hyperspectral data cubes in ENVI BIL format were provided in the form of radiance and atmospherically corrected reflectances. In addition to the 2013 hyperspectral data collection, the following imagery were collected during the LiDAR acquisition across the ACT in 2015:

- Visible 4-band (RGBI) imagery at 1 m resolution.
- Visible 3-band (RGB) imagery at 0.20 m resolution.
- Panchromatic visible imagery at 0.10 m resolution.

Hyperspectral data also appear to have been collected at Tumbarumba using a HyMap instrument, but a data description document was not available.

2.3.2 Preprocessing

The hyperspectral data collected by ARA were evaluated and preprocessed by Dr Arancha Cabello-Leblic (CSIRO) and Dr Lola Suarez (RMIT). The processing followed a protocol written by Mark Broomhall (Curtin University) that was subsequently published (Broomhall, Johansen and Wu 2015). The preprocessing included the following steps: (1) geographic correction, (2) atmospheric correction, (3) mosaicking, and (4) spectral convolution. Georeferencing was done to an accuracy of 1.5 m. All Vis-NIR data collected by the Eagle Sensor were available in reflectance units and were mosaicked. Achieving a reasonable signal-to-noise ratio required spectral convolution. The final image product has 121 spectral bands between 400 to 1000 nm, with a full width at half maximum of 10 nm.

However, this was not done for all SWIR data from the Hawk Sensor. The level of preprocessing is summarised in Table 4. Georeferenced and atmospherically corrected reflectances could be produced from the Eagle sensor Vis-NIR data for all ten sites, but this was only possible for 6 out of 10 sites with Hawk SWIR data.

Table 4. Preprocessing of the airborne hyperspectral data from the AusCover sites imaged by ARA.

	Eagle Sensor (VIR)				Hawk Sensor (SWIR)		
Site code	Georeferenced	Reflectance	Mosaic	Spectral convolution	Georeferenced	Reflectance	Mosaic
Cho	✓	✓	✓	✓	✓	×	×
Wat	✓	✓	✓	✓	✓	×	×
Rus	✓	✓	✓	✓	✓	×	✓
Zig	✓	✓	✓	✓	✓	×	✓
Cre	✓	✓	✓	✓	×	×	×
Rob	✓	✓	✓	✓	×	×	×
Sam/Kar/Wyn	✓	✓	✓	✓	✓	×	✓
Lit	✓	✓	✓	✓	✓	×	✓

A workshop between TERN and ARA on 26-27 November 2015 in Adelaide discussed the hyperspectral data quality and preprocessing workflow. The workshop identified quality issues with the hyperspectral data collected before September 2013, both in terms of georeferencing and radiometric quality. Inappropriate software was used for data

acquisition and processing, but the radiometric quality of the Eagle and Hawk instruments was generally good, although data calibration was not optimal.

No evaluation or information on preprocessing of the Tumbarumba data was available.

The quality of the ACT hyperspectral data was evaluated by Cabello-Leblic and Yebra (2014). They found that the real ground resolution achieved was 3.1–3.2 m and that 3 km^2 of one of the three locations (ACT02) were not collected. Furthermore, the mosaics they produced from the flight line data showed strong illumination artefacts. Those artefacts were not visible in the near-seamless mosaics provided by HyVista, and reflectance values were different. However, the contractor did not respond to requests for details on the processing steps to achieve this result. Furthermore, the provided data ranged from 470–2400 nm rather than 400–2500 nm as specified in the quotation. Finally, anomalous measurements were visible between 1380-1500 nm that were assumed to be due to atmospheric corrections.

3 PRODUCT REQUIREMENTS

3.1 INTRODUCTION

This section summarises the process followed to determine data priorities, summarises the results, and evaluates these against the quality and suitability of the LiDAR and hyperspectral data, and the current state of the art in deriving such data products.

The following summary of data priorities was based on discussion with a small sample of about 30 individuals drawn from TERN staff, remote sensing experts, ecologists, researchers and practitioners. It was assumed to provide a reasonable first overview of data requirements that can potentially be met with the airborne data that have been collected. A few general observations were made:

- The information needs of researchers and practitioners coincided quite well, and both groups shared a similar level of understanding of airborne data. This may partly be because the practitioners interviewed were relatively well connected to the research community, and partly because most of the researchers interviewed were not experts in remote sensing. Because the data priorities expressed aligned between research and management users, a distinction is not made here.
- A common theme was that the range of uses is limited by the lack of temporal sampling and, except for the ACT, the limited spatial extent of the data. This means that in many applications, direct use of the airborne data was not envisaged. Rather, its greatest use may be in the development or verification of data products derived from spatiotemporal remote sensing.
- In assessing priorities in data products, it was recognised that the ecosystem research community was the primary target audience for TERN. This held true even when constraining the analysis to the areas for which hyperspectral and LiDAR data was captured, with the latter in particular having potential applications in other fields. For example, the fields of geomorphology, water management, urban planning, agriculture, construction and renewable energy were all mentioned in the interviews. However, these were not considered priorities, except for where they happened to coincide with applications in ecosystem research and management.

- A few broad categories of data uses were identified, although there was considerable overlap between them, and alternative groupings can easily be made. These are discussed in the following sections. References are cited where they were mentioned by the interviewees and are not intended to represent a comprehensive review.

3.2 FUEL LOAD AND STRUCTURE

The utility of LiDAR data for fire risk mapping was most commonly mentioned by the interviewees. Partly this may reflect the author's network and the fact that ACT Government staff were well aware of the utility of LiDAR data for fuel characterisation. An important attraction was the potential to use LiDAR data in fuel hazard scoring systems that are amenable to quantitative spatial data. They include the Victorian assessment method widely known as the Fuel Hazard Score (Hines et al. 2010) that is also used in the ACT, and the 'Project Vesta method' (Gould et al. 2007). Despite inevitable differences, commonalities between the two systems include that they recognise:

1) Surface fuel (leaf litter, fine twigs, duff)
2) Near-surface fuel (typically herbs and grasses)
3) Elevated fuel (typically scrub)
4) Overstorey fuel, which can include a bark and canopy component (Hines et al. 2010) or consider an intermediate and top canopy separately (Gould et al. 2007).

Another commonality is that both methods describe field methods to assess fuel loads (in t/ha) that are based on transect or point sampling of the height or depth and the areal density cover of each fuel type, which is subsequently translated into a categorical five-tier score. A discussion and initial assessment of the use of LiDAR data for fire risk assessment was published by the Bushfire and Natural Hazards CRC (Yebra et al. 2015a). The review found that these field assessment methods appear very amenable to the use of LiDAR data, but there were some important caveats:

- The field assessment categorises strata by vegetation growth form, which is difficult to replicate with airborne LiDAR data, and are more easily stratified by height above ground of the returns. However, in practice field assessments also rely on a combination of height and growth form. For example, ACT Parks and Conservation uses heights of 50 cm and 200 cm as approximate bounds between near-surface, elevated and canopy fuels, respectively (A. Leavesley, ACT Parks & Conservation, pers. comm.).
- Due to common misclassification and small vertical errors of the last returns (i.e., originating from the soil or litter surface), the cover and structure of surface fuel cannot usually be reliably inferred.
- Field assessments distinguish between live and dead fuel, with is not possible to infer from single-frequency LiDAR.
- The infrequent or one-off acquisition of airborne LiDAR limits it uses to spatial prioritisation and classification, and prevents its use management more dynamic fuel components (e.g. herbaceous and fast-recovering scrub vegetation).

Notwithstanding these limitations, interviewees were very optimistic about the potential value of LiDAR-derived fuel information in their activities. In particular, the following suggestions were made about priorities:

- Fuel cover fraction in the surface, near-surface (<50 cm), elevated (50-200 cm) and canopy layer.
- Height of the top and base of the overstorey canopy.
- Spatial connectivity of fuel at different spatial scales

Examples of prospective uses of the data by practitioners included spatial prioritisation of prescribed burning and the identification of possible 'holding lines' (i.e. accessible lines with low fuel density) in the case of escaping or unplanned fire. Examples of prospective data use by practitioners included understanding fire risk in the urban-wildland interface, and fire spread modelling.

Fewer opportunities were identified for products that might be derived from the hyperspectral data, particularly given the one-off nature of data collection. However, some interviewees were aware of existing (NDVI-based) fuel moisture content monitoring systems based on operational satellite missions as well as systems currently in development, and appreciated the potential utility of the hyperspectral data to verify such systems.

3.3 VEGETATION STRUCTURE AND COMPOSITION, AND HABITAT

The use of airborne data for vegetation structure and habitat characterisation as well as species mapping was identified by several interviewees. Suggested uses varied considerably. Some examples that were mentioned include the spatial mapping of:

1) Vegetation stratification and density as an input to vegetation community mapping.
2) Vegetation communities (bogs) suitable to two particular amphibian species (corroboree frogs) based on landscape morphology and water detection.
3) Canopy species composition.
4) Invasive species (e.g., blackberry and pine) in conservation areas.
5) Large old trees, which are home to the large majority of tree hollows essential for many arboreal vertebrates and birds.
6) Coarse woody debris as a habitat for ground-dwelling fauna.
7) Canopy forage quality and biochemistry following Youngentob et al. (2012).

The lack of common metrics across these different examples demonstrates the difficulty of achieving standardised products that can meet these requirements, as will be discussed further in Section 3.6

3.4 URBAN VEGETATION

A third application area that was mentioned in the context of the ACT airborne data was the mapping and study of urban vegetation, specifically urban trees. In many ways, the information sought was similar to that mentioned in the previous section, but discussion with the interviewees indicated a greater emphasis on the location and dimensions (as well as species) of individual trees. The mentioned uses of these data were for urban fauna habitat assessment and the study of the impact of vegetation on liveability, respectively.

3.5 STANDING TIMBER VOLUME AND CARBON

A final application of the airborne data that was mentioned relates to the estimation of standing timber volume or total aboveground biomass. The two main applications of such data are in commercial forestry and carbon balance analysis. One of the explicit purposes of LiDAR acquisition by the ACT Government was to assess standing volume in its plantation forests (e.g., Kowen Forest), which has since been completed (C. Brack, ANU, pers.comm.). A closely related metric that is important for carbon studies is the total amount of aboveground biomass from which total dry matter and carbon stock can be derived.

The possible use of airborne LiDAR data to estimate timber volume or biomass was presented in two contrasting ways by the interviewees, namely: (1) using LiDAR-derived stock density and tree height to calculate volume or biomass using allometric equations; or (2) using LiDAR-derived biomass or timber volume to *derive* such allometric equations. Perhaps these two contrasting approaches reflect differences in the level of confidence in LiDAR-derived vegetation data when compared to allometric equations. A third application that is particularly relevant to carbon studies is the use of site-based estimates of aboveground biomass to calibrate or verify large-scale estimates of vegetation biomass derived from current or future satellite missions.

3.6 SPECIFICATIONS

Based on the preceding summary of consultation results, the feasibility of deriving relevant data products was analysed. The literature was surveyed for methods to derive ecosystem products. The feasibility of each of the published methods was analysed and compared to the usefulness given the indicated data priorities. In performing this analysis, the following criteria were considered:

1. *Published workflow*: Is there a sufficiently validated published data analysis method to derive the data product?
2. *Additional data dependencies*: Is the analysis possible given ancillary data or site calibration that may be required?
3. *Data quality*: Is the available data of sufficient quality to derive the product?
4. *Resources required*: Is the processing practically feasible given available resources?

Each of the criteria will be elaborated on below.

3.6.1 Published workflow

Only those products were considered for which a suitable published workflow or method exists, or can be derived by minor extrapolation of published work. The reasons for this were two-fold: (1) It was a contractual requirement that well-tested methods were to be used, rather than new research undertaken; and (2) the available time and resources were insufficient to develop new analysis methods.

3.6.2 Additional data dependencies

Many published methods to derive biophysical vegetation properties rely on the collection of field data simultaneously with airborne data collection to derive accurate spatial estimates. This is certainly true for purely statistical methods (e.g., regression) but also for conceptual or physically-based retrieval methods that require estimation of parameters. Where such dependencies exist, the method was not feasible and hence not considered. In some cases, it may be possible to use field data that was collected during the airborne campaign to derive a calibrated product. In such cases, the feasibility of deriving a lower level derived product that could be used for this purpose was considered. In other cases, the necessary ancillary data was not collected during the campaign.

3.6.3 Data quality

In assessing whether the available data were of sufficient quality to derive the identified potential products, some uncertain assumptions were made during the early stage of processing. These related to:

- the quality of the collected airborne data (e.g. the absolute accuracy of hyperspectral radiances and vertical accuracy of the LiDAR);
- the spatial density (i.e., the resolution of the hyperspectral data and pulse density of the LiDAR data);

- the quality of georeferencing and (co-)registration of the data;
- the spectral resolution and range of the hyperspectral data;
- the quality of preprocessing (e.g., the atmospheric correction and LiDAR discretisation and classification);
- the integrity, standard adherence and availability of metadata in the (preprocessed) data; and
- any other data quality aspects.

These assumptions considered in relation to the expected sensitivity of processing algorithms to data quality issues and lack of uniformity. For example, for the hyperspectral data, band ratios can often be calculated with good results, but absolute reflectances may not be of sufficient quality to be used. The characteristics and spatial variability of the surface and vegetation itself further determined product usability. In general, a 'user beware' approach was taken, that is, the products were generated and made available, but caveats need to be considered carefully when interpreting the products.

3.6.4 Resources required

A final important consideration were the resources required to process the data to the specified product. This includes the budgeted time and labour resources, as well as the required:

- high-performance computing time;
- connected data storage; and
- licensed or complex specialised processing software.

The opportunity to use licensed software was limited further by the ability to deploy it on the National Computational Infrastructure HPC resources. In assessing processing workflow feasibility, only Python or MatLab-based libraries for HPC-based processing were considered, but additional software was available for PC-based pre-or post-processing.

3.6.5 LiDAR products deemed infeasible

Some information requirements were expressed in the consultation but were considered infeasible, based on literature review and preliminary data exploration. These include, among others:

- *Delineation of tree crowns*. The mapping of tree crowns was tested using watershed segmentation methods (van Leeuwen and Nieuwenhuis 2010) and appeared to produce promising results where tree crowns did not overlap too much and were not severely clumped and thinned out (a feature of some old-growth eucalypt species). However, the processing would involve a large amount of computing resources and, in particular, would probably need fairly involved and site-specific tuning of the preprocessing and delineation workflow along with QA/QC. This was outside scope but could be considered in future work. Crown delineation could be undertaken for some test areas, however.
- *Standing volume or biomass*. The LiDAR data products derived likely make it possible to estimate standing timber volume or aboveground biomass, but a generic methodology or set of allometric equations is not available (van Leeuwen and Nieuwenhuis 2010). For individual sites, such equations can be derived from field data or the literature, but this would require site knowledge and a degree of judgement that was not available at this stage.
- *Species mapping*. LiDAR data has been used to map tree species based on crown form (van Leeuwen and Nieuwenhuis 2010). However, this requires the development of tree models. Moreover, the interpretation and supervised classification would require field knowledge of dominant species and possibly a training sample. This was outside scope but could be considered in future.

- *Coarse woody debris*. Although large logs have been identified in the LiDAR data, the pulse density is generally too low to classify even the largest logs reliably as separate from the ground layer. Moreover, mapping large woody debris requires an object-oriented delineation method. There are developments towards this in the literature (Wing et al. 2015), but at the time of writing there is no well-tested and scalable technique that could be employed. Alternative methods to estimate coarse woody debris involve empirical regression against other LiDAR metrics (Pesonen et al. 2008, Sumnall, Hill and Hinsley 2016). However, these require field data on coarse woody debris that can be used in empirical approaches.
- *Ground surface and litter characteristics*. In principle, the intensity and spread of the ground and near-ground returns might provide some indication of ground surface conditions or the amount of surface litter. In practice, the vertical errors appeared too great to analyse the vertical distribution reliably (particularly where flight lines overlap and at the edge of swaths). The energy intensity recorded with the ground returns did provide information on vegetation cover on the ground, particularly in open areas. However, such information is easily derived from hyperspectral imaging, and intensity information from the last return in dense vegetation was less easily interpreted.

3.6.6 Hyperspectral products deemed infeasible

Some information requirements were expressed in the consultation that were considered infeasible at this stage, based on literature review and preliminary data exploration. These include, among others:

- *Leaf area index.* Retrieving leaf area index (LAI) from hyperspectral data can be undertaken using either:
  i. an empirical approach that links vegetation indices (e.g., NDVI, FPAR or otherwise) to field-observed LAI; or
  ii. a conceptual approach that estimates LAI from vegetation canopy cover following a light extinction model such the exponential equation of Monsi and Saeki (1953); or
  iii. retrieving LAI from observation at multiple viewing angles.

  Method (iii) was not possible as only the (near-) vertical viewing angle imagery was available, whereas method (i) was not attempted as it would involve the use of field LAI observations. Method (ii) can be easily applied to the FPAR estimates (accounting for the assumption in FPAR that 5% of red light is reflected) or scaled EVI estimates. However, it requires an assumed extinction coefficient. Rather than assume a value, it was considered here that ecosystem researchers are typically aware of the conceptual relationship between LAI and canopy cover, and may have detailed knowledge about an appropriate coefficient value to use.

- *Species mapping*. Hyperspectral data has previously been used to map tree species based on spectral signature (Andrew and Ustin 2006, Asner and Martin 2008). However, similar to the mapping of species using LiDAR data (Section 3.6.5) this is only possible if species are spectrally very distinct and if ground data are available to relate species to spectral signature. This was out of scope, but researchers with site knowledge may be able to use the hyperspectral products for such a purpose.
- *Foliar chemistry.* For reasons explained in Section 5.4, it was not possible to derive foliar chemistry and composition reliably without additional sampling during airborne data collection. To the best of our knowledge, this was not undertaken, but if it was, then it may be possible to relate several of the spectral indices to observed spectral response. This process was out of scope.
- *Delineation of tree crowns*. Mapping tree crowns from hyperspectral data is possible if the crowns do not overlap or if the crowns of individual plants have a very different spectral signature. It is likely to be most successful if combined with LiDAR-based crown delineation (Section 3.6.5) which was out of scope.

4 LiDAR PRODUCTS

4.1 INTRODUCTION

To derive gridded LiDAR-based product, resampling individual returns to point densities in a regular grid is necessary. Considerations of the most appropriate grid resolution for the generated LiDAR products included:

1) Increasing spatial resolution leads to greater sample size and usually (though not always) reduces uncertainty in derived measures.
2) Gridded data at finer spatial resolution may be more cumbersome to view, download, store and process by users, and more expensive to host by TERN.
3) Resolution may need to match the scale of spatial variation that users wish to analyse. For example, the distribution of individual tree canopies may be the dominant scale of variation in open woodlands, whereas, in more uniform herbaceous or forest vegetation, topographical features may correspond to the scale of greatest variation.
4) Related to the above, the derived data may need to be combined with field assessments at a particular scale. For example, visual field assessment may encompass 100 m^2 or more, while more detailed measurements may involve a quadrat of less than one square metre or sampling of an individual tree.

It may be clear that there is unlikely to be a single grid size that fits all requirements, and so in practice, the first two considerations dominate. To provide flexibility around the last two considerations, data products were generated at three resolutions:

- The finest resolution that suits the pulse density and processing algorithm. It is assumed that this will typically be around 1 or 2 m.
- A resolution of 5m, which still produces a high-fidelity image for most sites (e.g., 1000 pixels over 5 km).
- A resolution of 25m, which is storage efficient and corresponds to the scale of rapid visual field assessment and the resolution of Geoscience Australia's Digital Earth Australia Landsat Data Cube.

The difference between the two grid resolutions is illustrated in Figure 3.

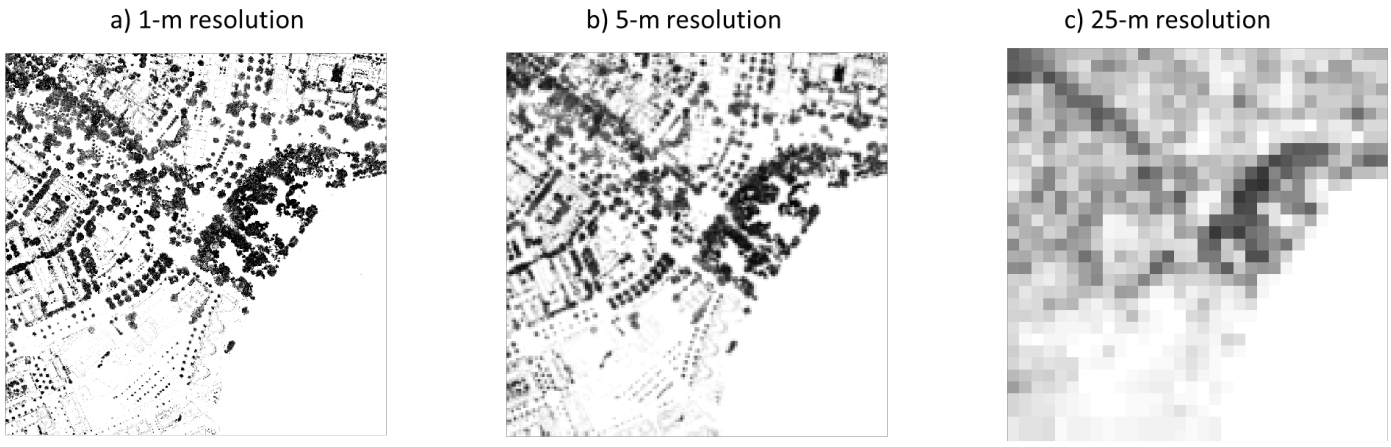

Figure 3. Canopy cover fraction calculated from >8ppm LiDAR data at the three different resolutions. The image covers 800m square around Telopea Park (ACT), chosen to illustrate the visibility of individual features.

4.2 VEGETATION HEIGHT (VH)

Vegetation height (VH in m) is readily retrieved from the first pulse returns that were classified as vegetation (van Leeuwen and Nieuwenhuis 2010). To calculate VH as height above the ground surface, the height of the first return above ground surface (*h*) were calculated by subtracting the ground elevation derived from a 1 m DEM from the elevation of the return (z). The main source of error is the inclusion of junk (erroneous) returns and incorrectly classified returns from objects above the vegetation (e.g., birds, power lines, buildings). Errors were reduced by calculating the median rather than the maximum of first return heights. Another source of error is the incorrect estimation of ground elevation, particularly in landscape parts with a very steep ground surface (e.g., gullies or rock faces) or where the DEM needed to be interpolated (e.g., water surface or building footprints). Both types of errors were reduced through averaging when resampling to a coarser resolution.

4.3 VEGETATION COVER FRACTION (VCF)

Vegetation cover fraction (VCF as a fraction) was calculated by considering how many of the first returns (N_{first}) were not from the 'solid' ground (Morsdorf et al. 2004):

$$VCF = \frac{N_{first} - N_{single}}{N_{first}}$$

Errors occur because of the surface footprint of the LiDAR (typically a few dm across) and because single returns may register even when there is vegetation on the surface (e.g. short grass). Therefore, VCF does not necessarily fully include vegetation cover on the ground and may have a bias compared to alternative ways of measuring canopy cover fraction. Finally, parts of the canopy other than leaves, such as branches, were included in the calculation of VCF, which may also be different compared to alternative measurements of canopy cover fraction.

4.4 CANOPY LAYERING INDEX (CLI)

A canopy layering index (CLI) was calculated by considering the total number of returns extracted for each pulse, and taking into account that the last return should represent the ground surface. Typically, only the first five returns were retained when producing discrete return data in LAS format, but the total number of returns of a pulse (*R*) was recorded as an attribute of each return point triplet. Using this information, the CCF was reconstructed in a slightly roundabout way as follows:

$$CLI = \frac{\sum w_R N_R R}{\sum w_R N_R} - 1$$

where N_R is the number of discrete return triplets for which the recorded number of total pulse returns equals *R,* and a relative weighting w_R is given by:

$$w_R = 1/min(N_R, 5)$$

The weight w_R was limited to that equivalent to five discrete returns, as additional returns for that pulse were not recorded. The CLI effectively represents the average number of discrete vegetation returns for the grid cell. While it is correlated with leaf area index (LAI), it is not identical to it (van Leeuwen and Nieuwenhuis 2010). Some of the reasons include:

1) partial leaf area within the pulse footprint can still lead to a full return being recorded;
2) LiDAR responds only to the (near-)horizontal leaf silhouette in the pulse beam;
3) leaves that are densely and evenly distributed with height may not produce separable peaks in the waveform;
4) woody canopy components can also generate returns that cannot be distinguished from those generated from the leaves; and
5) disregarding the last and single returns may ignore leaf area close to the surface.

Despite these differences, CLI and similar measures of vegetation layering have often been shown to correlate well with LAI, but some bias is likely. A generic method to estimate LAI reliably has not yet been demonstrated and cannot to be expected, given that the different biases depend on leaf size, orientation and clumping, as well as the LiDAR footprint and incidence angle.

4.5 VEGETATION LAYER COVER FRACTIONS (LCF)

For fuel risk assessment and vegetation characterisation, the degree of canopy cover in different vegetation strata is an important variable. An approximate estimate of the cover fraction for any vegetation layer was estimated by comparing the number of vegetation returns from a layer *L* between h_1 and h_2 (calculated as $N_{vh<h2} - N_{vh<h1}$) to the total number of vegetation returns from this layer plus the layers below it ($N_{vh<h1}$). This ratio quantifies the number of returns originating from layer L compared to the layers below it (Caynes et al. 2016). This approach mitigates the fact that returns from lower layers become less likely due to the interception from layers overhead (Caynes et al. 2016) and because a maximum of only five returns was only retained for each pulse. The calculation result did, however, need adjustment for the presence of uncovered surface, by multiplication with the actual overall vegetation cover fraction (VCF):

$$LCF = VCF\frac{N_{vh<h2} - N_{vh<h1}}{N_{vh<h2}}$$

Note that the sum of cover fractions in vertical layers can exceed the VCF, which can be interpreted as the result of super-positioned vegetation layers. These layer-specific canopy cover estimates are subject to the same types of uncertainties as those affecting the calculation of VCF and CLI (see Sections 4.3 & 4.4). A complicating factor is that the distinction between ground and vegetation returns is not always reliable at very low heights above surfaces, particularly in areas of overlapping flight lines. This introduces additional uncertainty for the lowest vegetation layers.

Another divergence with field assessments is that the vegetation returns are strictly classified by height. In field assessments, it is more likely that a visual distinction is made between plants with their canopy squarely within the designated layer, versus parts of plants that have their canopy primarily in another layer but may partly extend in the layer considered. Making this distinction was not feasible given the density of airborne LiDAR data and methods available, though such methods have been developed for terrestrial laser scanning (Marselis et al. 2016).

Following the method described above, LCF was calculated for any defined vegetation layer. For example, fuel assessment in the ACT uses the heights listed in Table 5 as a guideline. The 2-m boundary coincides with the minimum height of vegetation to be classified as forest following the National Carbon Accounting System definition (Furby 2002). By contrast, for vegetation community mapping in the ACT, vegetation layers are defined between 1–3 m (scrub) and >3 m height (trees) (G. Baines, ACT Parks & Conservation, pers. comm.). Other jurisdictions and users may use different definitions again.

Table 5. Fuel layer bounds as recognised by ACT Parks & Conservation (A. Leavesley, ACT Parks & Conservation, pers. comm.).

Fuel layer	Lower bound	Upper bound
Surface fuel (litter)	0 m	in contact with the ground
Near-surface fuel (standing fuel)	0 m	0.5 m
Elevated fuel	0.5 m	2.0 m
Canopy fuel	2.0 m	Canopy top

To accommodate this, LCF was calculated for the two different categorisations corresponding to two layer definitions with respective height bounds of

a) 0.05, 0.50, and 2.00 m; and
b) 0.05, 1.00, and 3.00 m.

4.6 Overstorey canopy top height (CTH)

Canopy top height (CTH) is another input when following the Victorian fuel assessment guide, but can also be useful for other purposes, such as tree crown delineation. CTH was calculated through a method very similar to vegetation height, but in this case, ignoring vegetation heights below 2 m height.

4.7 Overstorey canopy base height (CBH)

Canopy base height (CBH) is also an input when following the Victorian fuel assessment guide. Its definition can be more ambiguous: a plant may be classified as a tree because it extends more than 2 m, but that does not mean that its base also exceeds 2 m in height. This reflects the mentioned difference between classification based on growth form and height of the returns, respectively. For fuel classification, it is of particular importance to determine whether the base of the canopy is above the expected flame height or not, which is only likely the case if it is several metres above the elevated fuel layer. Therefore, a simplified approach was taken, whereby only the vegetation returns from above 2 m height were considered. Even then, there may be returns from woody tree components below the canopy base (e.g., trunk and main branches). To avoid these being included in the estimated canopy base height, the 10% quantile of the canopy returns was calculated.

4.8 Digital Elevation Model (DEM)

A DEM is required to derive many of the vegetation products, but is also a standard output of LiDAR preprocessing and is available for all areas covered at 1-m resolution. The DEM was reformatted and resampled to coarser resolutions as specified.

4.9 Fraction building footprints (FBF)

Building returns were classified separately in the LiDAR classification. A product of fraction building footprints (FBF) was derived from the data that may be useful in some applications. This product was only generated where building returns were identified.

5 HYPERSPECTRAL DATA PRODUCTS

5.1 INTRODUCTION

Similar as for the LiDAR data, different choices about grid resolution were made. In the case of the hyperspectral data, the preprocessed observations were already gridded. Each of the data products was produced at three different resolutions:

- The existing resolution of the preprocessed imagery. This was between 1-3 m.
- A resolution of 5 m, which still produces a high-fidelity image for most sites (e.g., 1000 pixels over 5 km).
- A resolution of 25 m, which is storage-efficient and corresponds to the scale of rapid visual field assessment and the resolution of the Geoscience Australia Digital Earth Australia Landsat Data Cube.

5.2 SIMULATED LANDSAT 8 OLI BAND REFLECTANCE

The hyperspectral data was convolved to Landsat 8 band reflectance using the corresponding response functions. These data are likely to be useful in algorithm development studies seeking to translate information developed at high-resolution or from hyperspectral data or both, to Landsat products or in similar comparative analyses. The spectral response functions of the Landsat 8 Operational Land Imager (OLI) (see Figure 4) were published by Barsi et al. (2014) and were available as a spreadsheet with relative response in 1 nm increments[2].

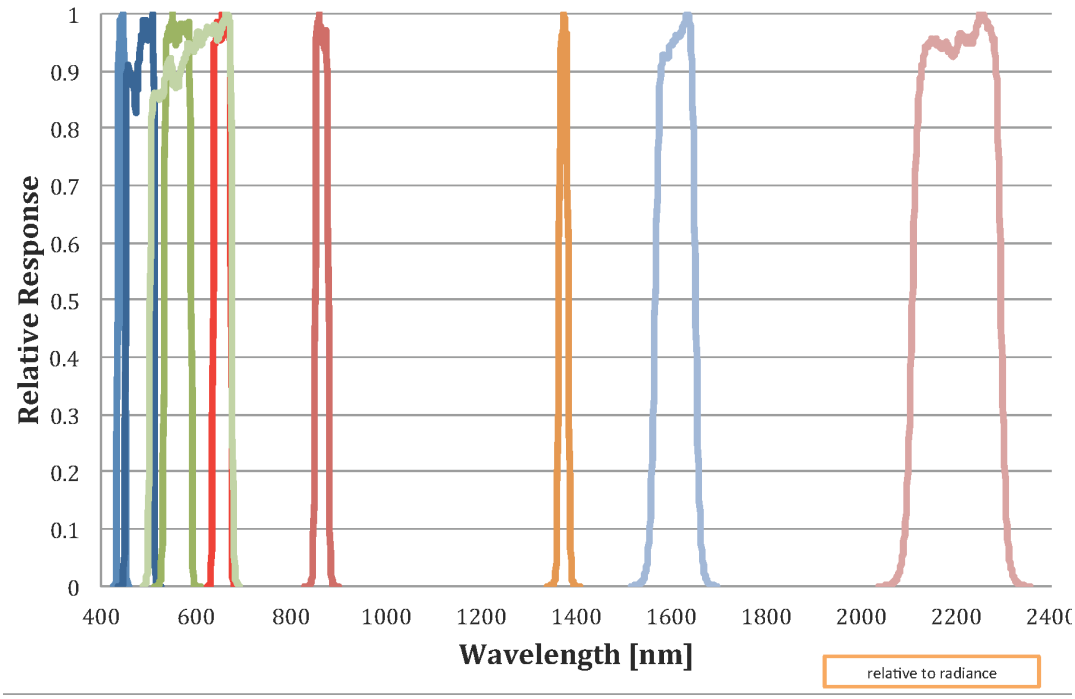

Figure 4. Response functions for the different Landsat 8 OLI bands.

[2] https://landsat.gsfc.nasa.gov/preliminary-spectral-response-of-the-operational-land-imager-in-band-band-average-relative-spectral-response/

Table 6. Approximate lower and upper limits of full width at half-maximum of each Landsat OLI band as well as the centre wavelength (all in nm). CA=coastal aerosol, NIR=near infrared, SWIR = shortwave infrared.

Band	lower	upper	centre
CA	434.97	450.95	442.96
Blue	452.02	512.06	482.04
Green	532.74	590.07	561.41
Red	635.85	673.32	654.59
NIR	850.54	878.79	864.67
SWIR1	1566.50	1651.22	1608.86
SWIR2	2107.40	2294.06	2200.73
Pan	503.30	675.70	589.50
Cirrus	1363.24	1383.63	1373.43

5.3 Simulated MODIS Band Reflectance

The hyperspectral data was also convolved to MODIS band reflectance using the corresponding response functions for the MODIS AQUA instrument[3]. Only bands that are used in terrestrial applications and that overlap with the hyperspectral measurements were calculated.

5.4 Foliage spectral indices

One of the primary purposes of hyperspectral data is the characterisation of foliage biochemistry using spectral features that correspond to specific constituents (e.g., pigments, lignin, cellulose and water). A challenge is to retrieve these measures from the hundreds of bands with reflectance values, the majority of which are highly correlated. One approach to process hyperspectral data is that of Youngentob et al. (2012), although this does not reduce the number of bands as such, and may also be sensitive to actual reflectance values and hence errors in measurement and preprocessing (e.g. atmospheric correction) as well as shading effects.

An alternative approach is to calculate spectral indices that have been designed to capture and enhance features in the spectral signature that are known to respond to physiologically meaningful parameters. An important advantage of many such indices is that they are based on ratios, which helps to remove the effect of bias, correction errors and shading. Andrew and Ustin (2006) reviewed and tested 19 such indices (Table 7).

Unfortunately, current methods to relate indices or any other hyperspectral data-derived information directly to physical units still require simultaneous and georeferenced field sampling followed by chemical analysis (Youngentob et al. 2012). Nonetheless, the indices listed in Table 7 can still provide information on the spatial patterns in the concentrations of certain constituents. This may be useful in understanding ecosystem function, or may possibly assist in species mapping.

[3] Available from https://mcst.gsfc.nasa.gov/calibration/parameters

Each of the indices in Table 7 were calculated using the collected hyperspectral data if the required reflectance data were available. This does not mean that all products are usable. For example, spatial patterns may be dominated by non-foliar materials, canopy shading, image acquisition or atmospheric correction artefacts. The user should consider this carefully in interpreting the products.

Table 7. Reflectance indices calculated from the hyperspectral reflectance data, where possible.

Indices	Formula	Details	Citation
Greenness indices			
Simple ratio (SR)	$RRED/RNIR$	Index of green vegetation cover. Various wavelengths used, depending on sensor (e.g., NIR = 845 nm, RED = 665 nm)	Rouse et al. (1974)
Normalised difference vegetation index (NDVI)	$\frac{(RNIR - RRED)}{(RNIR + RRED)}$	Index of green vegetation cover. Various wavelengths used, depending on sensor (e.g., NIR = 845 nm, RED = 665 nm),	Tucker (1979)
Summed green reflectance (SGR)	$\sum_{500}^{599} Rn$	Index of green vegetation cover	Fuentes et al. (2001)
Pigment indexes			
Modified NDVI (mNDVI)	$\frac{(R750 - R705)}{(R750 + R705)}$	Leaf chlorophyll content	Fuentes et al. (2001)
MERIS terrestrial chlorophyll index (MTCI)	$\frac{(R754 - R709)}{(R709 + R681)}$	Leaf chlorophyll content	Dash and Curran (2004)
Photochemical reflectance index (PRI)	$\frac{(R570 - R531)}{(R570 + R531)}$	Xanthophyll response to light photosynthetic efficiency. Also sensitive to Car/Chl ratio	Gamon et al. (1992)
Red/green ratio (RG)	$\frac{(R600 - R699)}{(R500 - R599)}$	Anthocyanins/chlorophyll	Fuentes et al. (2001)
Normalized pigments chlorophyll ratio index (NPCI)	$\frac{(R680 - R430)}{(R680 + R430)}$	Total pigments/chlorophyll	Penuelas, Baret and Filella (1995)
Simple ratio pigment index (SRPI)	$R430/R680$	Carotenoid/chlorophyll a content	Peñuelas et al. (1994)
Normalized phaeophytinization index (NPQI)	$\frac{(R415 - R435)}{(R415 + R435)}$	Chlorophyll degradation detects stress at early states	Barnes et al. (1992)

Indices	Formula	Details	Citation
Structure intensive pigment index (SIPI)	$\frac{(R800 - R445)}{(R800 - R680)}$	Carotenoid/chlorophyll a concentrations	Penuelas et al. (1995)
Pigment index 1 (PI1)	$R695 / R420$	Plant stress status	Zarco-Tejada (1998)
Pigment index 2 (PI2)	$R695 / R760$	Plant stress status	Zarco-Tejada (1998)
Pigment index 3 (PI3)	$R440 / R690$	Vegetation health based on chlorophyll fluorescence ratios	Lichtenthaler et al. (1996)
Pigment index 4 (PI4)	$R440 / R740$	Vegetation health based on chlorophyll fluorescence ratios	Lichtenthaler et al. (1996)
Water indexes			
Normalised difference water index (NDWI)	$\frac{(R860 - R1240)}{(R860 + R1240)}$	Leaf water content	Gao (1996)
Water band index (WBI)	$R900 / R970$	Leaf water content	Peñuelas et al. (1997)
Nutrient and dry matter content			
Normalized difference nitrogen index (NDNI)	$\frac{\log(R1860 - R1510)}{\log(1/R1860 \cdot R1510)}$	Foliar nitrogen concentration	Serrano, Penuelas and Ustin (2002)
Normalized difference lignin index (NDLI)	$\frac{\log(R1860 - R1754)}{\log(1/R1860 \cdot R1754)}$	Foliar lignin concentration	Serrano et al. (2002)
Cellulose absorption index (CAI)	$0.5(R2020 + R2220) - R2010$	Based upon cellulose and lignin absorption features; used to discriminate plant litter from soils	Nagler, Daughtry and Goward (2000)

5.5 Normalised Difference Vegetation Index (NDVI)

Although the normalised vegetation index (NDVI) (Tucker 1979) has no direct biophysical meaning, it is familiar to many ecosystem researchers and may be a useful product. NDVI was calculated as one of the hyperspectral indices mentioned above. It was also calculated from the simulated MODIS and Landsat 8 OLI band reflectance:

$$NDVI = \frac{NIR - Red}{NIR + Red}$$

where NIR and Red are the reflectances in the near-infrared and red bands, respectively.

5.6 Enhanced Vegetation Index (EVI)

Similar to NDVI, the Enhanced Vegetation Index has no direct biophysical meaning, but it closely related to measures of vegetation density, vigour and photosynthetic activity and familiar to many ecosystem researchers. EVI was developed to optimise the vegetation signal with improved sensitivity in biomass-dense regions and improved vegetation monitoring through decoupling of the canopy background signal and a reduction in atmosphere influences (Huete et al. 2002). It was calculated from the simulated MODIS band reflectance as follows:

$$EVI = \frac{2.5(NIR - Red)}{NIR + 6Red - 7.5Blue + 1}$$

Where NIR, Red and Blue are the reflectances in the near-infrared, red and blue bands, respectively.

The coefficients of this equation are calibrated for MODIS band reflectances, and therefore EVI was not calculated from the simulated Landsat 8 OLI band reflectance.

5.7 Fraction of absorbed Photosynthetically Active Radiation (FPAR)

In principle, the fraction of photosynthetically active radiation absorbed by vegetation (FPAR) can be calculated from hyperspectral observations following detailed, physically based approaches. However, this requires spectral observations of coincident incoming radiation and knowledge of sensor-sun geometry. Because the data only represent a one-off observation under transient atmospheric and surface conditions, a simple approach was considered more appropriate, and a linear ramp function was applied to the simulated MODIS NDVI following Donohue, Roderick and McVicar (2008). Rather than the AVHRR-based NDVI of Donohue et al. (2008), the version developed for MODIS by Yebra et al. (2015b) was used:

$$FPAR = 0.95 \times \max\left(min\left(\frac{NDVI-0.1}{0.9-0.1}, 1\right), 0\right)$$

This ramp function increases linearly from 0 for NDVI ≤ 0.1 to 0.95 at NDVI ≥ 0.9.

5.8 Global Vegetation Moisture Index (GVMI)

Similar to the Normalised Difference Water Index (NDWI, Table 7) another commonly used vegetation moisture content indices is the Global Vegetation Moisture Index (GVMI), which was calculated from MODIS band reflectance as (Ceccato, Flasse and Gregoire 2002):

$$GVMI = \frac{(NIR + 0.1) - (SWIR2 + 0.1)}{(NIR + 0.1) + (SWIR2 + 0.1)}$$

where SWIR2 represents MODIS reflectance at 1640 nm.

5.9 Open Water Likelihood (OWL)

The presence of open water can usually be mapped fairly accurately based on short-wave reflectance or even the magnitude of negative NDVI values. Maps of the area of open water were produced by calculating Open Water

Likelihood (OWL), applying the additive logarithmic regression model of Guerschman et al. (2011) to the simulated MODIS band reflectance. It is given by:

$$OWL = \frac{1}{1 + exp(-z)}$$

where *z* is a coefficient calculated as the sum of linear terms of several explanatory variables *x* as:

$$z = \beta_0 + \sum \beta_i x_i$$

Out of 36 candidate models, Guerschman et al. chose the following fitted model version:

$$z = -3.4138 - 0.0009\,SWIR2 + 0.0042\,SWIR3 + 14.1928\,NDVI - 0.4304\,NDWI - 0.0961\,MrVBF.$$

where SWIR2 and SWIR3 are the shortwave bands centred around 1600 nm and 2200 nm, respectively, NDWI is defined in Table 7, and MrVBF is the Multiresolution Valley Bottom Flatness (MrVBF) index (Gallant and Dowling 2003) derived from the national 3-second DEM derived from the Shuttle Radar Topography Mission data. To avoid the use of MrVBF, a value of MrVBF=1 was assumed. Subsequently, areas of the landscape that are highly unlikely to have open water were masked by threshold classification based on the LiDAR DEM.

5.10 Crop coefficient (Kc)

The empirical algorithm developed by Guerschman et al. (2009) was applied to the simulated MODIS band reflectance to calculate an equivalent 'crop coefficient' (Kc), which predicts evapotranspiration rate as a fraction of potential evapotranspiration. Under conditions without rainfall, it is given by:

$$K_c = K_{c,max}[1 - \exp(-2.482 EVI_r^{2.482} - 7.991 RMI^{0.890})]$$

where scaled EVI_r is a ramp function, such that EVI_r=0 for $EVI \leq 0$ and EVI_r=1 for $EVI \geq 0.9$, and the Residual Moisture Index (RMI) is calculated as:

$$RMI = max(0, GVMI - 0.775 EVI + 0.076)$$

5.10.1 Penman-Monteith Surface Conductance (PMSC)

The empirical approach used to estimate surface conductance for use as a parameter in the Penman-Monteith model (PMSC) was developed by Yebra et al. (2013) by applying an exponential equation to three different vegetation vigour indices (NDVI, EVI and Kc) and taking the average of three predictions of PMSC (G_s) from each of three indices (VI):

$$G_s(VI) = a\ \ exp[b(VI - VI_{min})]$$

The coefficients *a*, *b* and VI_{min} have been optimised against global flux tower data, producing the values listed in Table 8.

Table 8.Parameter estimates to estimate surface conductance following Yebra et al. (2013).

VI	a	b	VI_{min}
NDVI	2.0	4.11	0.4
EVI	2.5	3.15	0.1
Kc	0.3	5.14	0

REFERENCES

Andrew, M. E. & S. L. Ustin (2006) Spectral and physiological uniqueness of perennial pepperweed (Lepidium latifolium). *Weed Science,* 54**,** 1051-1062.

ARA. undated. AusCover Data Report (unpublished).

Asner, G. P. & R. E. Martin (2008) Airborne spectranomics: mapping canopy chemical and taxonomic diversity in tropical forests. *Frontiers in Ecology and the Environment,* 7**,** 269-276.

Barnes, J., L. Balaguer, E. Manrique, S. Elvira & A. Davison (1992) A reappraisal of the use of DMSO for the extraction and determination of chlorophylls a and b in lichens and higher plants. *Environmental and Experimental botany,* 32**,** 85-100.

Barsi, J., K. Lee, G. Kvaran, B. Markham & J. Pedelty (2014) The Spectral Response of the Landsat-8 Operational Land Imager. *Remote Sensing,* 6**,** 10232.

Broomhall, M., K. Johansen & D. Wu. 2015 Quality Assurance Steps for AusCover Hyper-Spectral Data. In *AusCover Good Practice Guidelines: A technical handbook supporting calibration and validation activities of remotely sensed data product,* eds. A. Held, S. Phinn, M. Soto-Berelov & S. Jones, 249-260. TERN AusCover.

Cabello-Leblic, A. & M. Yebra. 2014. Hyvista hyperspectral data quality evaluation report. CSIRO, ANU, TERN.

Caynes, R. J. C., M. G. E. Mitchell, D. S. Wu, K. Johansen & J. R. Rhodes (2016) Using high-resolution LiDAR data to quantify the three-dimensional structure of vegetation in urban green space. *Urban Ecosystems,* 19**,** 1749-1765.

Ceccato, P., S. Flasse & J. M. Gregoire (2002) Designing a spectral index to estimate vegetation water content from remote sensing data-Part 2. Validation and applications. *Remote Sensing of Environment,* 82**,** 198-207.

Dash, J. & P. J. Curran (2004) The MERIS terrestrial chlorophyll index. *International Journal of Remote Sensing,* 25**,** 5403-5413.

Donohue, R., M. Roderick & T. McVicar (2008) Deriving consistent long-term vegetation information from AVHRR reflectance data using a cover-triangle-based framework. *Remote Sensing of Environment,* 112**,** 2938-2949.

Fuentes, D. A., J. A. Gamon, H. l. Qiu, D. A. Sims & D. A. Roberts (2001) Mapping Canadian boreal forest vegetation using pigment and water absorption features derived from the AVIRIS sensor. *Journal of Geophysical Research: Atmospheres,* 106**,** 33565-33577.

Furby, S. 2002. Land Cover Change: Specification for remote sensing analysis. In *National Carbon Accounting System - Technical Report*. Canberra: Australian Greenhouse Office.

Gallant, J. C. & T. I. Dowling (2003) A multi-resolution index of valley bottom flatness for mapping depositional areas. *Water Resources Research,* 39**,** 1347-1360.

Gao, B.-C. (1996) NDWI—A normalized difference water index for remote sensing of vegetation liquid water from space. *Remote sensing of environment,* 58**,** 257-266.

Gould, J. S., W. McCaw, N. Cheney, P. Ellis & S. Matthews. 2007. *Field guide: fuel assessment and fire behaviour prediction in dry eucalypt forest*. Commonwealth Scientific and Industrial Research Organization (CSIRO).

Guerschman, J., W. Garth, G. Byrne, L. Lymburner, M. Norman & A. I. J. M. Van Dijk. 2011. MODIS-based standing water detection for flood and large reservoir mapping: algorithm development and applications for the Australian continent. Canberra, available at http://www.clw.csiro.au/publications/waterforahealthycountry/wirada/TechReports/WIRADA-MODIS-standing-water.pdf: CSIRO.

Guerschman, J. P., A. Van Dijk, G. Mattersdorf, J. Beringer, L. B. Hutley, R. Leuning, R. C. Pipunic & B. S. Sherman (2009) Scaling of potential evapotranspiration with MODIS data reproduces flux observations and catchment water balance observations across Australia. *Journal of Hydrology,* 369**,** 107-119.

Hines, F., K. G. Tolhurst, A. A. G. Wilson & G. J. McCarthy. 2010. *Overall fuel hazard assessment guide*. Victorian Government, Department of Sustainability and Environment.

Huete, A., K. Didan, T. Miura, E. P. Rodriguez, X. Gao & L. G. Ferreira (2002) Overview of the radiometric and biophysical performance of the MODIS vegetation indices. *Remote Sensing of Environment,* 83**,** 195-213.

Johansen, K. undated. AusCover Supersite and Data Information (http://wiki.auscover.net.au/w/images/5/58/AusCover_Site_Information5.pdf). Remote Sensing Research Centre / Joint Remote Sensing Research Program, School of Geography, Planning and Environmental Management, The University of Queensland.

Lichtenthaler, H., M. Lang, M. Sowinska, F. Heisel & J. Miehe (1996) Detection of vegetation stress via a new high resolution fluorescence imaging system. *Journal of plant physiology,* 148**,** 599-612.

Marselis, S. M., M. Yebra, T. Jovanovic & A. I. van Dijk (2016) Deriving comprehensive forest structure information from mobile laser scanning observations using automated point cloud classification. *Environmental Modelling & Software,* 82**,** 142-151.

Monsi, M. & T. Saeki (1953) Über den Lichtfactor in den Pflanzengesellschaften und seine Bedeutung für die Stoffproduktion. *Japanese Journal of Botany,* 14**,** 22-52.

Morsdorf, F., E. Meier, B. Kötz, K. I. Itten, M. Dobbertin & B. Allgöwer (2004) LIDAR-based geometric reconstruction of boreal type forest stands at single tree level for forest and wildland fire management. *Remote Sensing of Environment,* 92**,** 353-362.

Nagler, P., C. Daughtry & S. Goward (2000) Plant litter and soil reflectance. *Remote Sensing of Environment,* 71**,** 207-215.

Penuelas, J., F. Baret & I. Filella (1995) Semi-empirical indices to assess carotenoids/chlorophyll a ratio from leaf spectral reflectance. *Photosynthetica,* 31**,** 221-230.

Peñuelas, J., J. Gamon, A. Fredeen, J. Merino & C. Field (1994) Reflectance indices associated with physiological changes in nitrogen-and water-limited sunflower leaves. *Remote sensing of Environment,* 48**,** 135-146.

Peñuelas, J., J. Pinol, R. Ogaya & I. Filella (1997) Estimation of plant water concentration by the reflectance water index WI (R900/R970). *International Journal of Remote Sensing,* 18**,** 2869-2875.

Pesonen, A., M. Maltamo, K. Eerikäinen & P. Packalèn (2008) Airborne laser scanning-based prediction of coarse woody debris volumes in a conservation area. *Forest Ecology and Management,* 255**,** 3288-3296.

Rouse, J., R. Haas, J. Schell, D. Deering & J. Harlan (1974) Monitoring the vernal advancement and retrogradation (green wave effect) of natural vegetation. *NASA/GSFC Type III Final Report, Greenbelt, Md,* 371.

RPS - Mapping. 2016. Final Report: Acquisition of LiDAR and Imagery for the Australian Capital Territory. 18. RPS.

Serrano, L., J. Penuelas & S. L. Ustin (2002) Remote sensing of nitrogen and lignin in Mediterranean vegetation from AVIRIS data: Decomposing biochemical from structural signals. *Remote sensing of Environment,* 81**,** 355-364.

Sumnall, M. J., R. A. Hill & S. A. Hinsley (2016) Comparison of small-footprint discrete return and full waveform airborne lidar data for estimating multiple forest variables. *Remote Sensing of Environment,* 173**,** 214-223.

Tucker, C. J. (1979) Red and photographic infrared linear combination for monitoring vegetation. *Remote Sensing of Environment,* 8**,** 127-150.

van Leeuwen, M. & M. Nieuwenhuis (2010) Retrieval of forest structural parameters using LiDAR remote sensing. *European Journal of Forest Research,* 129**,** 749-770.

Wing, B. M., M. W. Ritchie, K. Boston, W. B. Cohen & M. J. Olsen (2015) Individual snag detection using neighborhood attribute filtered airborne lidar data. *Remote Sensing of Environment,* 163**,** 165-179.

Yebra, M., S. Marselis, A. Van Dijk, G. Cary & Y. Chen. 2015a. *Using LiDAR for forest and fuel structure mapping: options, benefits, requirements and costs*. Bushfire & Natural Hazards CRC, Australia.

Yebra, M., A. Van Dijk, R. Leuning, A. Huete & J. P. Guerschman (2013) Evaluation of optical remote sensing to estimate actual evapotranspiration and canopy conductance. *Remote Sensing of Environment,* 129**,** 250-261.

Yebra, M., A. I. Van Dijk, R. Leuning & J. P. Guerschman (2015b) Global vegetation gross primary production estimation using satellite-derived light-use efficiency and canopy conductance. *Remote Sensing of Environment,* 163**,** 206-216.

Youngentob, K. N., L. J. Renzullo, A. A. Held, X. Jia, D. B. Lindenmayer & W. J. Foley (2012) Using imaging spectroscopy to estimate integrated measures of foliage nutritional quality. *Methods in Ecology and Evolution,* 3**,** 416-426.

Zarco-Tejada, P. (1998) Optical Indices as Bioindicators of Forest Sustainability: Research Evaluation Course. *Toronto, Canada: York University*.